

# Chemical zoning and open system processes in the Laacher See magmatic system

Emma L. Tomlinson, Victoria Smith, Martin M. Menzies

## Abstract

Unraveling the generation of compositionally and thermally zoned magma reservoirs is important to our understanding of the dynamic processes operating in magmatic systems. Here, we present new major and trace element data for volcanic glasses from the classically zoned Laacher See Tephra and suggest that mafic recharge may play an important role in producing the observed compositional gradient. Mafic phonolite glass from the upper part of the Laacher See Tephra records the addition of ca. 30% basanite magma, which is recognised by an increase in REE+Y and a decrease in Th, U and Zr relative to glasses from more evolved units. We suggest that the Laacher See magmatic system was sustained by repeated episodes of basanite recharge and calculate a recharge magma flux of between  $2 \times 10^{-5}$  and  $1 \times 10^{-4} \text{ km}^3 \text{ y}^{-1}$  in the 20kyr leading up to the eruption. Basanite addition would have provided heat required to generate the strong compositional and thermal gradients that are recorded in crystals ejected during the Laacher See Tephra eruption.

**Key words:** Magmatic system, mafic recharge, phonolite, compositional zoning, trace element.

## 1. Introduction

Explosive volcanic eruptions commonly emplace chemically zoned deposits that are the inverted contents of chemically and thermally stratified magma chambers. Well-known examples include the large rhyolite tuffs from the western USA, such as the Bishops Tuff (Hildreth and Wilson 2007), Ammonia Tanks Tuff (Deering et al. 2011) and Carpenter Ridge Tuff (Bachmann et al. 2014)) as well as smaller alkali pyroclastic successions such as the Pantelleria Green Tuff (Liszewska et al. 2018), Neapolitan Yellow Tuff (Forni et al. 2018) and the Laacher See Tephra (Wörner and Schmincke 1984a). One of the major questions in igneous geology concerns the processes that lead to zoning in these magmatic systems. Possible end-member mechanisms include closed system processes such as extended fractionation of resident magma (e.g. Wörner and Schmincke 1984b; Bacon and Druitt 1988) and crystal accumulation (e.g. Deering et al. 2011) and open system processes, such as the injection of one or more magma pulses that do not undergo significant mixing, variable degrees of mixing between resident and incoming magma batches (e.g. Eichelberger et al. 2000) or melting of cumulate minerals (Wolff et al. 2015).

Unraveling the mechanisms that generate chemical zoning is fundamental to our understanding of the internal structure and dynamic processes operating in magmatic systems. Extended fractionation in a closed system is central to long-lived conceptual models that view magma chambers as coherent bodies of magma, however such models are being revised in the light of geochemical data, geochronological data and numerical models. Variations in crystal chemistry and zoning indicate that magmatic systems show temporal and spatial variability in both melt composition and temperature (Ginibre et al. 2004b; Humphreys et al. 2006; Smith et al. 2009) as well as being subject to extensive open system processes (Degruyter et al. 2016; Ganne et al. 2018). Thus, both fractionation and mafic recharge are likely to contribute to compositional zoning in magmatic systems. The relative roles of crystal fractionation and mafic recharge may also be an important control on magma storage

conditions within the crust. In some, particularly longer lived magmatic systems, absolute crystal ages are significantly older than their diffusion ages suggesting that they have spent a significant proportion of their lifetime at near solidus conditions within a crystal mush (Cooper and Kent 2014). In such cases, mafic recharge shortly before eruption may have led to melting and ‘rejuvenation’ of the crystal mush to form an eruptible volume of magma (Bachmann and Bergantz 2009). In other magmatic systems, magma melt bodies have been maintained over extended timescales (Barboni et al. 2016), numerical models indicate that a high rates of magma recharge are critical to maintaining liquid melt bodies (Annen 2009; Solano et al. 2012). Thus, current models view magmatic systems as reservoirs containing a volume of eruptible magma, extracted from melt pockets within an associated crystal mush and subject to repeated inputs of fresh magma (see reviews by Bachmann & Huber 2016 and Cashman et al. 2017).

The Laacher See Tephra (LST) is considered to be an archetypal continuously zoned magma chamber, varying from cool, crystal-poor evolved phonolite at the top to hotter, crystal-rich mafic phonolite at the base (Wörner and Schmincke 1984a). Chemical zonation within the LST has been attributed to extended fractional crystallisation of mafic phonolite (Wörner and Schmincke 1984b; Tait et al. 1989). However, individual LST sanidine crystals show complex changes in melt chemistry and large internal temperature variations (Ginibre et al. 2004b), which suggest more complex processes were operating the LST system. In this contribution, we present micron-beam major and trace element data for magmatic glasses from the LST showing that the system was not linearly zoned but rather displays abrupt compositional steps. We re-examine the evolution of the magmatic system in the light of this new glass data and demonstrate an important role for periodic basanite recharge in producing compositional zoning in the LST.

## 2. Geological Background

Laacher See volcano is located in East Eifel Volcanic Field (EEVF) of western Germany, part of the Cenozoic alkaline intraplate volcanic province of central Europe that produced basanites, leucites and nephelinites and their differentiated products from ca. 100 eruptive centers during the past 440 ka (Duda and Schmincke 1987). The  $12,880 \pm 40$  cal. yrs BP (Bogaard and Schmincke 1985; Brauer et al. 1999; Baales et al. 2002; Litt et al. 2003) eruption of Laacher See was the most recent event in the EEVF. The LST was erupted into a depression occupied by Quaternary basanitic spatter and scoria cones and lava flows and the eruption excavated a 2.5km diameter crater which is now filled with a lake. With an erupted magma volume of  $6.3 \text{ km}^3$  (Harms and Schmincke 2000) and a volcanic explosivity index of  $\sim 5$  (Newhall and Self 1982), the Laacher See tephra was one of the most violent eruptions in Europe in the last 20 ka and tephra deposits from the LST eruption blanket central Europe (Bogaard and Schmincke 1985). The LST eruption generated a complex sequence of Plinian, phreato-Plinian and phreatomagmatic deposits that include pyroclastic falls, flows and surges (Bogaard and Schmincke 1984). The LST stratigraphy is sub-divided into three main units based on stratigraphy and composition: the Lower (LLST), Middle (MLST) and Upper (ULST) Laacher See Tephra units. Juvenile LLST tephra is composed of nearly aphyric, highly differentiated phonolite magma. The MLST tephra is composed of grey, weakly porphyritic phonolite, which becomes more mafic and porphyritic with height in the stratigraphy. Juvenile ULST fragments are grey and highly porphyritic with mafic phonolite glass. The juvenile clasts become progressively more mafic and crystal-rich with height in the stratigraphy, and co-mingled phonolite-basanite clasts are present in late-erupted ULST (Wörner and Wright 1984).

Sanidine is the dominant phenocryst throughout the LST sequence, followed by plagioclase, hauyne, amphibole, clinopyroxene, titanite, Ti-magnetite, apatite and phlogopite. The proportions of mafic minerals, such as clinopyroxene, amphibole and biotite, are highest in the ULST (Wörner and Schmincke 1984a). In addition, nepheline and zircon are found in the LLST. A number of cumulate nodules are also found in the LST units, varying from mafic (dominated by clinopyroxene, amphibole, magnetite and apatite) through intermediate, with equal proportions of mafic and felsic minerals (clinopyroxene, amphibole, mica, apatite, titanite, plagioclase and sanidine), to felsic (dominantly sanidine with subordinate orthoclase), these are most common in the uppermost MLST and in ULST deposits but occasionally found in earlier erupted products (Tait et al. 1989; Schmitt et al. 2010). In addition, syenite-carbonatite (calcite sanidine and noselite) nodules are interpreted as the cool carapace of the LST magma reservoir rather than as cumulate nodules (Tait et al. 1989; Schmitt et al. 2010; Rout and Wörner 2018).

Wörner & Wright (1984) describe co-mingled phonolite-basanite juvenile clasts within the late erupted portion of the ULST. These clasts vary in texture from dense and poorly vesicular through to pumiceous. Phonolite derived phenocrysts, such as sanidine, sodic plagioclase, hauyne, and amphibole have evolved melt inclusions, and show inverse zoning and resorption textures. Phenocrysts from basanite melts, such as olivine and magnesian clinopyroxene, are also present the mingled clasts and exhibit normal zoning (Wörner and Wright 1984). These observations indicate that the lowermost portion of the LST magma reservoir mixed with a basanitic magma shortly before eruption (Wörner and Wright 1984).

The LST exhumed and entrained a significant proportion of metamorphosed and fenitized lithic fragments during eruption (10-40% of the erupted volume in fall layers, 90% in phreatomagmatic layers) (Bogaard and Schmincke 1984). The country rock xenoliths reflect the stratigraphy of the crust that hosted the LST magma reservoir, which comprises Lower Devonian sedimentary rocks and intercalated Tertiary sediments to a depth of 3-5km, overlying a basement composed of phyllites and mica schists (Bogaard and Schmincke 1985).

### 3. Methods

The LST stratigraphy was sampled at a quarry near Mendig (50°23.555N, 7°16.576E), 2.5km south of the volcanic depression in the Laacher See basin. Vesicular juvenile clasts were collected from fall layers (LLST and MLST) and flows (ULST) to represent the compositional range in the magma chamber (Fig. 1). In addition, basanitic lithic clasts recovered from the ULST deposits were analysed along with a sample of the Rothenburg basanite (East Eifel), which are used to represent the local basanite composition in mixing calculations.

#### 3.1 Electron microprobe

Micron-scale major element compositions of LST glasses were analysed using Jeol8600 electron microprobe, equipped with 4 wavelength dispersive spectrometers and SamX software, at the Research Laboratory for Archaeology and the History of Art, University of Oxford. An accelerating voltage of 15kV, low beam current (6nA), and defocused (10µm) beam were used to minimize Na migration. Count times were 30 s on each peak, except for Na (10 s) and P and Cl (60 s). The instrument was calibrated for the beam conditions using a suite of appropriate mineral standards and count rates were corrected using the PAP absorption correction method. The calibration was verified using a range of reference glasses (MPI-DING) from the Max Planck Institute (Jochum

et al. 2006). Repeated analysis of these reference glasses indicates that precision is <10% relative standard deviation (%RSD) for analyses with concentrations >0.8 wt%.

### 3.2 Laser Ablation Inductively Coupled Plasma Mass Spectrometry

LA-ICP-MS analyses of proximal tephra samples were performed using an Agilent 7500es coupled to a Resonetics 193nm ArF excimer laser-ablation system (RESolution M-50 prototype) with a two-volume ablation cell at the Department of Earth Sciences, Royal Holloway University of London. We used a 25µm spot, a repetition rate of 5Hz and a count time of 40 s (200 pulses) on the sample and 40s on the gas blank (background). Concentrations were calibrated using NIST612 with <sup>29</sup>Si as the internal standard. Data reduction was performed manually using Microsoft Excel allowing removal of portions of the signal compromised by the occurrence of microcrysts. Full details of the analytical and data reduction methods are given in Tomlinson et al. (2010). Accuracies of ATHO-G and StHs6/80-G MPI-DING glass analyses are typically <5% for most elements and <10% for Nb, Pr, Eu, Gd, and Ta. Reproducibility of ATHO-G and StHs6/80 analyses is <5 RSD% for all trace elements, and relative standard errors (%RSE) for sample tephra LA-ICP-MS analyses are typically <5 %RSE for all elements.

### 3.3 Solution ICP-OES/MS

Basanite samples were digested and analysed at Royal Holloway University of London. 20 mg of powdered sample was mixed with 1g LiBO<sub>2</sub> powder in a graphite crucible, and then fused at 950°C in a muffle furnace. The molten bead was then dissolved in 200 ml of 5% HNO<sub>3</sub>. Solutions were analysed for major elements using a Perkin Elmer Optima 3300RL ICP-OES with an Echelle spectrometer and a segmented-array charge-coupled-device detector. Trace elements were analysed using an Agilent 7500 quadrupole ICP-MS. Quality control standards were BHVO-1 and GBW07312 with accuracies better than 5%.

## 4. LST melt compositions

Representative glass compositions are given in Table 1, the full dataset is provided in the Supplementary Information. LST glasses are phonolitic, with high normative nepheline (10-33%), in agreement with previous studies (Wörner and Schmincke 1984a, b). The micron-beam glass data reported here are more evolved than the whole-rock compositions reported by Wörner & Schmincke (1984a) and Wörner et al. (1983) and the difference can be accounted for by incorporation crystals in the whole rock analyses (calculated using the average compositions and relative abundances of phenocrysts) with the exception of Nd in the LLST for which some published whole rock values are higher than the bulk composition calculated from glass composition and phase abundance. LST glasses have SiO<sub>2</sub> concentrations that span a relatively narrow range (56.8-60.0 wt% in the LLST and MLST and constant in the ULST), therefore we use CaO as a differentiation index (Fig. 2). The most incompatible elements in the LST tephra are enriched by 10-1000 x primitive mantle, with negative Ba, Sr and Eu anomalies and U-shaped rare earth element (REE) patterns (Fig. 3), implying roles for feldspar and amphibole in LST petrogenesis. Concentrations of Rb, Nb, Zr, U, Th increase from ULST to LLST, herein we use Zr as a differentiation index in trace element plots. There are striking variations in major and trace element concentration between the least and most evolved magmas, with CaO decreasing from 7.5 to 0.4 wt%, Zr increasing >5x from 360 to 2000 ppm, and Ba decreasing >100 fold from 890 to 2.6 ppm.

The LLST melt is the most evolved portion of the LST. Concentrations of CaO, MgO, TiO<sub>2</sub>, Na<sub>2</sub>O and V are constant. Elements readily partitioned into sanidine (Al<sub>2</sub>O<sub>3</sub>, K<sub>2</sub>O, SiO<sub>2</sub>) are more variable and extend to both higher and lower concentrations than observed in the MLST. Incompatible elements are highly enriched, up to 1400 x primitive mantle and the normalized plot shows strong enrichments in Rb, Th, U, Nb and Zr, a U-shaped REE profile (La/Sm<sub>N</sub> = 33-39) and negative anomalies in Sr, Ba and Eu (Eu/Eu\* = 0.40-0.48) (Fig. 3). Elements involved in feldspar fractionation (Sr, Ba, Rb) are correlated. The High Field Strength Elements (HFSE; Th, Zr, Nb, Ta, Y and the Rare Earth Elements (REE)) and Rb are inter-correlated, with values plotting along straight lines on bivariate plots (Fig. 4).

MLST glasses span a narrow compositional range, with minor decreases in MgO, FeO, TiO<sub>2</sub> and V and increases in Al<sub>2</sub>O<sub>3</sub>, Na<sub>2</sub>O and K<sub>2</sub>O with decreasing CaO. MLST glasses have feldspar related anomalies in Ba-Sr-Eu (Eu/Eu\* = 0.43-0.5) and a U-shaped REE profile (La/Sm<sub>N</sub> = 29-39) (Fig. 3). MLST glasses have similar Nb-Th-U-Zr-Rb inter-element ratios to the LLST at lower overall concentrations. However, MLST glasses have higher ratios of REE+Y to Zr, forming trends that are offset from the LLST glasses. Therefore, there is a step change in composition between the LLST and MLST (Fig 4).

The ULST is the least evolved unit of the LST, as denoted by its higher CaO content. There is a compositional gap between the MLST and the ULST in both major elements (e.g. observed in CaO between 0.45 and 1.50 wt% and Na<sub>2</sub>O between 7.8 and 10.0 wt%) and trace elements (Zr 600-880 ppm; Rb 260-370 ppm; Th 21-31 ppm) (Fig. 2, 4). Major element variation within the ULST is limited, with slight decreases in CaO, MgO, FeO and TiO<sub>2</sub> and increases in Al<sub>2</sub>O<sub>3</sub>, Na<sub>2</sub>O and K<sub>2</sub>O; SiO<sub>2</sub> is constant at 60.1±0.7 wt%. ULST glasses lack the strong enrichment in the highly incompatible elements Th, U, Nb and Zr seen in the LLST and MLST glasses, and these elements do not project through the origin in variation diagrams (Fig. 4). ULST glasses have minor feldspar-related anomalies (Ba, Sr, Eu) with Eu/Eu\* = 0.87-1.04. The U-shaped REE pattern is less pronounced in the ULST glasses than in the LLST and MLST (La/Sm<sub>N</sub> = 12-23) (Fig. 3) and concentrations of the MREE (Pr, Nd, Dy, Er)+Y extend to high concentrations at constant or possibly slightly decreasing Zr (Fig. 4).

The basanite clasts found in the LST deposits have higher Ba and Sr than the ULST mafic phonolite, with 1142 ppm Ba and 866 ppm Sr (Fig. 4), and are similar to those in the East Eifel range that have 1032-1229 ppm Ba and 709-1036 ppm Sr (Wörner et al. 1983a; Gluhak and Hofmeister 2009). The basanites do not have a U-shaped REE pattern, and have higher MREE (Pr, Nd, Dy, Er) and Y relative to La than observed in the ULST (Fig. 3) giving La/Sm<sub>N</sub> = 4.3.

## 5. Discussion

Phonolite is the end product of fractionation on the basanite series (Coombs and Wilkinson 1969). Petrogenesis of phonolite via fractional crystallisation of clinopyroxene, amphibole, Ti-magnetite, feldspar, apatite and titanite (± olivine and mica) from basanite has been modeled (Wörner and Schmincke 1984b; Le Roex et al. 1990) and demonstrated experimentally (Irving and Green 2008). Extensive fractionation of amphibole would lead to MREE depletion and the development of concave upwards REE patterns in the residual melt (e.g. Irving and Price 1981). Wörner & Schmincke (1984b) proposed that the mafic LST phonolite formed by ~70% fractionation of basanite magma and that this mafic phonolite is parental to the LST magma series (Wörner and

Schmincke 1984b). The pressure at which the LST magma last equilibrated has been estimated at 100-200 MPa based on comparisons between whole rock compositions and the Ne-Ksp-Qz system (Wörner and Schmincke 1984b). Phase equilibria experiments on the LLST indicate that this was stored at 145 MPa (Harms et al. 2004), corresponding to a depth of 5km for the top of the LST magma system.

The LST records a steep temperature gradient. Equilibration temperatures for the LLST have been estimated to be 750–760 °C on the basis of amphibole compositions (Harms et al. 2004) and 720±20°C based on the TiO<sub>2</sub> concentration of melts (Berndt et al. 2001) produced in phase equilibria experiments. Individual feldspar crystals from the LLST record a wide temperature range, from ~800°C to as low as 650°C based on variations in anorthite content, suggesting possible thermal disequilibrium between minerals and melt (Ginibre et al. 2004b). The temperature range between the LLST and the ULST is estimated to have been between 120 and 140°C at the time of the eruption (Berndt et al. 2001). However, zoning patterns in feldspar phenocrysts present a more complex picture, with individual crystals from the ULST recording temperature variations of up to 300°C over their crystallisation history based on variations in anorthite content observed within single crystals (Ginibre et al. 2004b).

## 5.1 LST magma differentiation

The LST represents the inverted contents of a compositionally and thermally zoned magma reservoir. The development of zoning is traditionally attributed to either 1) in situ fractional crystallization; or 2) magma mixing/mingling. Furthermore, accumulation of crystals is likely to be an important process; in view of the observation that the least evolved magma composition (the ULST) has the highest crystal content. The role of each of these processes in the evolution of the LST is examined below. In particular, we focus on processes taking place within the ULST portion of the LST magmatic system.

### 5.1.1 Fractionation and accumulation

In the seminal work of Wörner & Schmincke (1984b), LST petrogenesis was attributed to fractionation of the most mafic melt (i.e. equivalent to the whole rock composition of the ULST phonolite) and the agreement between the predicted and observed phase abundance, composition and crystallization sequence supports a key role for fractionation. We can further test whether simple fractionation of mafic phonolite can reasonably explain full range of compositional variation within the LST by using Rayleigh fractionation [using  $C_i/C_0 = F^{D-1}$ ; where  $D$  is the bulk partition coefficient,  $X_i$  is the modal fraction of a given mineral and  $D_i$  is the bulk partition coefficient for element  $i$ ] to estimate the degree of crystal fractionation and mineral proportions that are required to produce the most evolved LLST magma (Supplementary Information). We investigate the fractionation of sanidine and plagioclase feldspar, which together account for >90% of the fractionated mineral assemblage of the LST. We use Ba and Sr as markers of sanidine and plagioclase and the mineral-melt partition coefficients of (Fedele et al. (2015). The Rayleigh fractionation modelling indicates that the MLST and LLST require 27-40% and 35-45% fractionation of feldspar from the least evolved ULST glass composition to produce the observed range in Ba (3-887 ppm) and Sr (3-663ppm) within the LST glasses. A higher degree of feldspar crystallisation is suggested by whole rock major element mass balance modeling by Wörner & Schmincke (1984b), who calculate that the MLST and LLST evolved from the ULST by 57-76% and ~80% fractionation of an assemblage

comprising ~85-90% feldspar. Therefore, there is a discrepancy between the degree of fractionation indicated by major and trace elements.

## **LLST**

Sanidine is the dominant phenocryst in the crystal-poor (<5 vol.%; Wörner and Schmincke 1984a), highly evolved phonolite magma of the LLST. These crystals have a composite structure comprising a sanidine host with intergrown albite lamellae, interpreted to reflect growth at the solvus (Ginibre et al. 2004b). Using the measured concentration of Sr and Ba in the LLST glasses (4-24 ppm and 6-18 ppm, respectively) and partition coefficients ( $D_{Sr}$  and  $D_{Ba}$ ) of 5, we calculate equilibrium concentrations of 20-120 ppm Sr and 30-90 ppm Ba in LLST sanidine. This is in agreement with reported sanidine compositions (Wörner et al. 1983a; Ginibre et al. 2004b) and indicates that many of the sanidine phenocrysts are in equilibrium with their host LLST magma.

Both trace (this study) and major element (Wörner and Schmincke 1984b) variation within the LLST can be accounted for by 5-10% fractionation of feldspar±amphibole from the least fractionated LLST composition. The phase assemblage is consistent with phase equilibria experiments on the LLST magma, where magnetite was the liquidus phase, followed by amphibole and then sanidine below 775°C (Harms et al. 2004). The modeled degree of crystallisation is significantly higher than the observed phenocryst abundance, indicating that a portion of the LLST crystals were effectively removed from the magma via settling or crystallisation on the chamber walls.

## **MLST**

The MLST layer varies from highly evolved phonolite to more mafic phonolite (Wörner and Schmincke 1984a), with a concomitant increase in phenocryst content from 2-5% to 10-15% (Wörner and Schmincke 1984a). Sanidine is the main phenocryst within the MLST, however plagioclase also becomes an abundant phase especially towards the base of the MLST. MLST sanidine crystals display a range of morphologies, with resorbed grains and also composite and pseudo-oscillatory zoned crystals comparable to those in the LLST and ULST, respectively (Ginibre et al. 2004b). Sr and Ba concentrations in the MLST glasses vary from 6 to 31 ppm and 8 to 36 ppm and sanidine in equilibrium with this melt should have 53-270 ppm Sr and 112-500 ppm Ba, calculated using the  $D_{Sr}$  and  $D_{Ba}$  values Fedele et al. (2015). However, reported sanidine compositions span a wider range (Wörner et al. 1983a; Wörner and Schmincke 1984b; Ginibre et al. 2004b). The composite, resorbed and some pseudoscillatory zoned sanidines formed in equilibrium with more evolved melt, while other pseudoscillatory crystals also formed in equilibrium with less evolved melt (Supplementary data S2). The limited MLST plagioclase trace element data is in equilibrium with a melt that is more mafic than the MLST. Using measured MLST glass compositions and the  $D_{Sr}$  and  $D_{Ba}$  values Fedele et al. (2015) of we calculate that plagioclase in equilibrium with the MLST melt has up to 465 ppm Sr and 68 ppm Ba - significantly lower than the reported Sr (~3200 ppm) and Ba (~930 ppm) compositions of the MLST plagioclase crystals (Wörner et al. 1983a). The MLST feldspars are not in trace element equilibrium with their host melt (Wörner et al. 1983a), plagioclase may have crystallised within the ULST melt, and a significant portion of sanidine crystals erupted within the MLST were originally from the LLST and ULST.

Trace element variation within the MLST can be accounted for by ~16% fractionation feldspar±amphibole from the least fractionated MLST composition. This modeled phase assemblage is comparable to that produced during MLST phase equilibria experiments in which biotite and sanidine crystallised with or without magnetite and/or hauyne (Berndt et al. 2001); it is likely that biotite stabilised at the expense of amphibole due to the higher

temperature conditions used by Berndt et al. (Harms et al. 2004). The modeled degree of crystallisation is at the high end of the observed phenocryst content of the MLST. The modeled proportion of crystallisation is lower than the degree of crystallization predicted by whole rock major element mass balance modeling (46% crystallisation from 1050 to 1026, of which ~85% feldspar; Wörner and Schmincke 1984b). There is also a discrepancy between the degree of crystallisation required for the transition between the MLST and ULST predicted by trace and major elements. Rayleigh fraction modelling of Ba and Sr indicates that the difference between the most evolved ULST glass (Sr = 118 ppm, Ba = 173 ppm) and the least evolved MLST glass (Sr = 31 ppm, Ba = 36 ppm) can be accounted for by 13% crystallization of feldspar. In contrast, whole rock mass balance by Wörner and Schmincke (1984b) suggests that 33% fractionation of an assemblage of 78% feldspar is required explain the difference in major element composition. While differences in the predicted degree of crystallisation within the MLST and between the MLST and ULST can be, in part, accounted for by the effect of crystal accumulation on the whole rock major element mass balance calculations and by differences in the exact stratigraphic positions of sample collection, the ULST to MLST transition is the main source of the difference in the degree of crystallisation across the LST calculated from major and trace elements.

### *ULST*

The ULST is a mafic phonolite whose phenocryst content rapidly increases from 25% to an average of 50-60 vol.% (Wörner and Schmincke 1984a). The dominant phenocryst is sanidine (~50 vol.%), followed by plagioclase (~25 vol.%) with lesser amounts (ca. 5-10 vol.%) of amphibole, clinopyroxene, hauyne and trace amounts (<3 vol.%) of titanite, magnetite, phlogopite and apatite (Wörner and Schmincke 1984a). Several lines of evidence suggest a role for crystal accumulation in the evolution of the ULST. Phase equilibria experiments using a ULST whole-rock starting composition crystallised clinopyroxene, plagioclase and biotite (or amphibole; Harms et al. 2004) with only minor alkali feldspar (Berndt et al. 2001), which contrasts to the large proportion of sanidine in ULST tephra. In addition, sanidine crystals present in the ULST vary from those in chemical equilibrium with the host ULST magma to those in equilibrium with a more evolved melt (supplementary data; also Wörner et al. 1983a; Ginibre et al. 2004b). Thus, it appears that a significant portion of the ULST phenocryst population represents crystals formed higher in the magmatic system. Accumulation can account for the lower than expected phenocryst abundances in the LLST and MLST layers, and the conversely higher than expected phenocryst content and sanidine abundance in the ULST, and for the observation that many crystals within the ULST are in equilibrium with less evolved (LLST- and MLST-like) melt.

Rayleigh fractionation modelling within the ULST (from the least to the most evolved ULST glass composition) suggests that 15% fractionation of feldspar is required to explain the variation in Ba and Sr within the ULST glasses, comparable to the proportion of feldspar fractionation within the ULST predicted through via whole rock major element mass balance modeling (20% crystallisation of which 85% feldspar; Wörner and Schmincke 1984b). Rayleigh fractionation modeling of clinopyroxene and amphibole fractionation within the ULST is problematic because of the influence of titanite, which controls the distribution of REE+HFSE and has a preference for the MREE over the LREE and HREE (Wörner et al. 1983a; Olin and Wolff 2012). ULST glasses form a triangular distribution in REE+Y content, with a trend towards high REE+Y at intermediate Zr contents. One possible explanation for the range of REE contents in ULST glasses is fractionation of titanite within the ULST. We investigate the potential influence of titanite fractionation from the ULST glass with the highest MREE concentrations using the titanite-phonolite partition coefficients of Olin and Wolff (2012), which are similar to the values of Wörner et al. (1983a) but constrained by the lattice strain model and cover a wider range



of elements. Starting at the ULST with the highest concentrations of MREE, fractionation of titanite causes a sharp decrease in REE+HFSE at decreasing Zr and Nb (Fig 5a-d): fractionation of 0.5% titanite is required to explain the range in the most compatible elements (the MREE + Ta), while crystallisation of 4x as much titanite (2%) is required to produce the range in the LREE and HREE, although the titanite fractionation does not give a good fit for the LREE+HREE. When titanite is considered as part as a fractionating assemblage of feldspar+clinopyroxene+amphibole (85:8:3), titanite must make up 10-15% of the fractionating assemblage in order that the bulk partition coefficients are high enough to produce the trend of decreasing REE in the ULST. This proportion of titanite is rather high, indeed whole rock major element mass balance of the ULST indicates that titanite made up 0.15% of the fractionating assemblage (Wörner and Schmincke 1984b). In addition, fractionation of titanite does not explain the triangular distribution of the REE+Y elements that extends to higher and lower Zr within the ULST, or the stepped compositional changes observed between the ULST and MLST and the MLST and LLST. Therefore, we suggest that, although fractionation of titanite clearly occurred in the ULST, as demonstrated by the presence of titanite phenocrysts, titanite fractionation did not cause the upward swing in the MREE+Y observed within the ULST glasses.

### 5.1.2 Basanite mixing in the ULST

The triangular distribution of trace elements implies that more than one process may have been operating during the evolution of the ULST magma: fractionation of the ULST magma from low to high Zr, and the addition of an REE-rich component. This is supported by the observation that, when plotted on variation diagrams, highly incompatible (Rb-U-Th-Zr) trace elements define linear trends that do not point towards the origin in the ULST (Fig. 4g,h), contrary to what is expected for fractional crystallisation alone.

One possible explanation for the elevated REE+Y and less steeply convex upward REE profile in the ULST relative to the MLST+LLST is the addition of REE-bearing phases, such as amphibole, clinopyroxene and/or titanite, to the ULST and, importantly, their subsequent resorption within the fractionating ULST melt. However, the REE+Y are enriched during fractionation of the MLST and LLST, suggesting that significant amounts of these elements are not being removed from the MLST and LLST and added to the ULST. For this reason, trace element modeling of the compositional variation in the fractionating MLST liquid and concomitant crystal residue is unable to produce a suitable mixing end-member for the ULST (Fig. 5e-f). Therefore, we exclude significant resorption of REE-bearing phenocrysts formed in the MLST and LLST as the source of REE enrichment in the ULST. Assimilation of amphibole-bearing crustal rocks as the source of REE+Y enrichment in the ULST is considered unlikely because accidental lithic fragments within the LST are mainly composed of amphibole-free rocks: phyllite and mica schist basement overlain by a range of sedimentary rocks (Bogaard and Schminke 1984). Furthermore, minimal assimilation of crustal rocks is indicated by the mantle-like oxygen isotope compositions of LST zircons (Schmitt et al. 2010) and by the  $^{87}\text{Sr}/^{86}\text{Sr}$  compositions of ULST and MLST phenocrysts, which overlap with the parental basanite (Wörner et al. 1985; Ginibre et al. 2004a).

The occurrence of mingled basanite-phonolite juvenile clasts within the ULST suggests a potential role for earlier episodes of basanite recharge during the evolution of the LST magma reservoir. Starting with a parental mafic phonolite with a U-shaped REE profile, the addition of basanite would increase the REE+Y concentrations in the hybrid melt. Importantly, the ULST glasses and whole rocks extend towards comingled basanite-phonolite clasts (Wörner and Wright 1984) for all trace elements, including the REE+Y (Fig. 4). Relative to the ULST

mafic phonolite, basanites from the East Eifel region have lower concentrations of U and Th and lack trace element anomalies relating to fractionation of feldspar (Ba, Sr, Eu). Therefore, mixing of basanite would lead to a decrease in U+Th and increases in REE+Y and Sr+Ba, though the latter may be obscured by the competing effect of feldspar fractionation. To test the hypothesis of mixing/replenishment of the ULST by basanite magma, we plotted a compatible element (V) against a highly incompatible element (Th). Mixing of melts would produce data that plot along a straight line, whereas fractional crystallisation of the melt would produce a hyperbolic trend, with its curvature reflecting the difference between the bulk distribution coefficient of the elements being considered. The ULST fractionation curve was calculated using the fractionating assemblage calculated by (Wörner and Schmincke 1984b), and because bulk partition coefficients vary by four orders of magnitude ( $D_V = 3$ ,  $D_U = 0.0003$ ) the resulting trend is a strongly curved hyperbola. We calculate the fractionation trend from the least evolved ULST glass at a range of  $D_V$  values, since this value is sensitive to the proportion of magnetite in the fractionating assemblage (Fig. 6). The ULST glasses span a narrow range in both compatible and highly incompatible elements, and the data lie on both a the straight portion of the calculated fractionation hyperbola and a mixing line between fractionating ULST and basanite (Fig. 6b) hampering the recognition of mixing and/or fractionation on these plots. However the ULST glasses appear to define a straight line in U-Th, V-V/Th and also on the companion plot  $1/V-V/Th$ , this demonstrates that the geochemical variation of U and V are at least compatible with a mixing scenario.

To test the effect of mixing on the incompatible element composition of the ULST melt, we have modeled simple mixing between ULST phonolite and basanite using incompatible element ratio plots. For mixing end-members we use the composition of the Rothenburg basanite and two possible starting compositions for the ULST: The ULST glass with the lowest MREE+Y (LS10-3) and a hypothetical mafic phonolite parental magma calculated from trace element biplots by projecting the MLST and LLST glass trends back to 500 ppm Zr where the ULST trend intersects the MLST+LLST trend. In a two-component system, mixing is linear if the denominators of the ratios are the same. Intermediate points along the hyperbola indicate the relative proportions of each end-member and therefore should lie on a straight line on a companion plot of one of the original ratios versus the ratio of the denominators of the two original ratios (Langmuir et al. 1978). The ULST glasses plot on the calculated mixing line between basanite and the hypothetical mafic phonolite, within individual samples recording approximately constant basanite proportions across all elements (Fig. 7). Basanite mixing increases the concentrations of the MREE+HREE+Y in the ULST glass, and may slightly dilute concentrations of Rb, Nb, La, U and Th however mixing is competing with fractionation for these elements. Variation in ULST glass composition is explained by addition of up to 40% basanite to the least mixed ULST glass, however this value is a minimum as it assumes no basanite was added to sample LS10-3. The distribution of values indicates that the ULST was not fully hybridised, possibly because mixing was inhibited by the rigid crystal framework of the ULST. The average proportion of basanite added to the ULST is 30%, this value is the net total and may have accrued over several recharge episodes.

Regardless of the relative timing of basanite addition and melt separation within the magmatic system, the glass compositions indicate that at least one episode of basanite recharge may have occurred during differentiation of the LST magma, this prior to and distinct from the recharge event that occurred shortly before the onset of the LST eruption (Wörner and Wright 1984). Published Sr-isotope values can be used to evaluate whether the model of 30% basanite mixed into the ULST. The Sr-isotopes values of the matrix glass and phenocrysts vary between 0.7048 and 0.7075 with highest values occurring in the LLST (Wörner et al. 1985), this trend was interpreted as

the result of late-stage contamination of the LLST by the original authors. In contrast, Ginibre et al. (2004a) suggest that assimilation occurred heterogeneously, on the basis that radiogenic compositions are not restricted to low-Sr differentiated sanidines, but also occur in the cores of some less differentiated sanidines and in sanidines from the main magma body. We suggest an alternative scenario in which the radiogenic Sr compositions of the LLST are the result of the assimilation of 1-2% mica schist during the early evolution of the LST magma system, and that the trend towards lower  $^{87}\text{Sr}/^{86}\text{Sr}$  in the less differentiated portions of the LST reservoir reflects subsequent mixing of East Eifel basanite. We have calculated mixing lines between basanite (800ppm Sr, 0.7047  $^{86}\text{Sr}/^{86}\text{Sr}$ ) and the most radiogenic LST compositions for matrix glass using the data of (Wörner et al. 1985) we do not use the phenocryst and whole rock data of (Wörner et al. 1985) because of the effect of crystal accumulation and mixing on the bulk composition, and also because the whole rock values do not lie between the matrix and phenocryst values as expected. The composition of ULST matrix glass (sample 1060) can be replicated with ~32% basanite addition to the most radiogenic magma (Supplementary data), which is in agreement with the proportion of basanite estimated using trace elements. While this estimate is based on only a small number of available Sr-isotope data points, it demonstrates that, at the very least, these data are consistent with basanite mixing.

Mafic recharge is also consistent with the pseudo-oscillatory zoning that is observed in the ULST sanidines, in which internal resorption surfaces reflect heating and destabilization of sanidine and decreasing Ca contents across growth zones indicate renewed sanidine growth during cooling (Ginibre et al. 2004b). The calculated temperature difference across internal resorption surfaces is significant (up to 300°C; Ginibre, Wörner, et al. 2004) and consistent with the intrusion of basanite melt at ca. 1060°C (Wörner and Wright 1984). Pseudo-oscillatory zoned sanidines also show compositional zoning (Ti, Ba and Sr) reflecting variations in the composition of the equilibrium melt (Ginibre et al. 2004b). The occurrence of pseudo-oscillatory zoning in LST sanidines was attributed to convection within the compositionally and thermally and compositionally zoned LST magma chamber by the original authors, however it may also be explained by mixing between the hypothetical ULST starting composition and hotter basanite magma. In this scenario, the quasiperiodic nature of zoning in ULST sanidines indicates that basanite recharge was episodic. Indeed, the occurrence of one or two high-volume basanite recharge events is not consistent with the low average storage temperatures of feldspar crystals from the cool outer carapace of the LST magma reservoir, however the storage temperatures do not exclude short duration, low magnitude heating and cooling events (Rout and Wörner 2018). Thus episodic addition of small batches of basanite magma is preferred to a single high-volume intrusion event. Indeed, images of pseudo-oscillatory sanidines in Ginibre et al. (2004b) suggest that these particular grains record 5-10 recharge events.

## 5.2 Structure of the magmatic system and differentiation of the LST melts in the upper crust

The LST magma evolved via crystallisation of sanidine, plagioclase, hauyne, amphibole and clinopyroxene (Wörner and Schmincke 1984b; Berndt et al. 2001), leading to the accumulation of crystals forming a crystal mush. We suggest that crystal-melt fractionation within the crystal mush was the main differentiation process, facilitated by intermediate crystallinity of the ULST, which is within the optimal range for crystal-liquid separation identified by Dufek and Bachmann (2010). We propose that during crystallization, numerous batches of crystal poor melt were released from a mush zone. Each batch rose to its own appropriate level in the melt-buoyancy gradient, the LLST pooling higher in the system than the MLST. We envisage that the LLST and MLST stalled to form separate melt pockets within crust (Fig. 8), however the LLST and MLST could also be

interpreted as separate melt pockets within a single magma reservoir. These segregated melts then continued to evolve, undergoing a further 15-20% fractionation of an assemblage dominated by sanidine, much of which settled and accumulated at the edge of the melt pocket and augmenting the crystal mush. During eruption, the accumulated crystals became entrained in ascending magmas from deeper in the magmatic system, LLST crystals in the MLST and MLST crystals in the ULST.

In a departure from previous models that view the LST as a closed fractionating system, we suggest an alternative model in which the ULST crystal mush was subject to periodic recharge by basanite magma forming a hybridised intermediate phonolite-basanite, which continued to differentiate. Mixing between basanite and phonolite within the ULST is likely to have been inhibited by the high crystallinity of the crystal mush, leading to the heterogeneous distribution of basanite within the ULST. Mass transfer of basanite to the MLST and LLST melts was minimal to absent, so these portions of the LST magma mush have been isolated from the recharge, possibly because they were stored at higher levels within the crust, were not affected by recharge events deeper in the magmatic system. The MLST may have been affected by localized movements of some ULST melt as there are some ULST-sourced phenocrysts within the MLST deposits. Recent seismological work revealed a possible feeder channel extending from 10 to 40km beneath the Laacher See Volcano and indicates that magmatic recharge of crustal reservoirs below Laacher See volcano is ongoing (Hensch et al. 2019).

### 5.3 Effect of basanite recharge

Recharge by hot, mafic magma shortly before eruption is suggested to play an important role in generating chemical zoning by inducing partial melting of the crystal mush, as documented in the Carpenter Ridge Tuff (Bachmann et al. 2014) and the Neapolitan Yellow Tuff (Forni et al. 2018). Injection of mafic magma also adds heat to the lower part of the magma reservoir and so generates the thermal gradients, which are observed in the deposits. Late intrusion of mafic magma into the ULST melt also occurred prior to the Laacher See Tephra eruption, as evidenced by mingled basanite-phonolite clasts (Wörner and Wright 1984). Addition of basanite at 1060°C (Wörner and Wright 1984) likely contributed to the strong thermal gradient within the LST. (Wolff et al. 2015) argue that mafic recharge events induced melting of the LST crystal cumulate, forming an intermediate cumulate melt and contributing to compositional zoning of the LST. Interestingly, Wolff et al. (2015) note that the composition of the ULST is not equivalent to a cumulate cognate with the most evolved magma as it is more strongly enriched in incompatible elements, and this observation is consistent with modification of the cumulate composition by recharging magma. However, the ULST glasses lack the positive Eu anomaly that would be expected to result from significant feldspar dissolution (Fig. 3).

This work additionally highlights the importance of earlier episodes of mafic intrusion in generating extreme compositions and chemical zoning as incoming mafic magma hybridizes with resident magma in the crystal mush. Furthermore, periodic input of basanite may also have sustained a persistent thermal gradient within the upper crust. Experiments demonstrate that chemical zoning may be generated by crystallisation along a thermal gradient, as the degree of crystallisation and melt composition vary with temperature (Masotta et al. 2012). This process allowed the full range of magma compositions to be produced by crystal-melt fractionation within the crystal mush. We suggest that episodic basanite recharge into the LST system drove compositional zoning both by augmenting the ULST melt in the crystal mush and by driving differentiation along a thermal gradient within the LST magmatic system.

U-series dating of mineral separates from evolved cumulates (Bourdon et al. 1994) and of zircons and within cogenetic carbonatitic and syenitic nodules (Schmitt 2006; Schmitt et al. 2010) record LST differentiation as far back as 32.6 ka, with a major episode at 17ka. Differentiation requires crystal-liquid separation, which itself implies the presence of melt, thus the LST magma reservoir must have existed for ca. 20 ka or at least 4 ka prior to eruption. Based on a volume of 1.3km<sup>3</sup> for the ULST (eruption volume estimated from Harms and Schmincke (2000)) and the modeled results that suggest 30% of the melt was originally basanitic in composition, we suggest that a net total of 0.4 km<sup>3</sup> basanite was added to the LST magma reservoir during this time span. We calculate a basanite recharge rate of 2x10<sup>-5</sup> km<sup>3</sup>y<sup>-1</sup> for the LST magma reservoir based on an age of 20 ka, which increases to 1x10<sup>-4</sup>km<sup>3</sup>y<sup>-1</sup> if we assume a younger age of 4ka for the magmatic system. Assuming that the rate of magma recharge reflects the overall magma flux that led to the development of the parental intermediate phonolite, these values are within range of the minimum magma flux required to sustain an eruptible magma volume of 6.3 km<sup>3</sup> within the upper crust, estimated as 6x10<sup>-3</sup> km<sup>3</sup>y<sup>-1</sup> and 8x10<sup>-5</sup> km<sup>3</sup>y<sup>-1</sup> by extrapolating the numerical models of Annen, (2009) and Gelman, Gutiérrez and Bachmann (2013), respectively, to lower magma volumes and correspondingly shorter magma residence times. Thus, episodic basanite recharge is considered a likely, mechanism for sustaining the LST magma reservoir.

The volume of the final recharge event recorded as mingled clasts is likely to be of the order of 0.05-0.1 km<sup>3</sup> (assuming 20% of the ULST was affected by this basanite addition and a basanite content of 20-40% in mingled clasts). Approximately 4-8 recharge events of similar magnitude may have occurred during differentiation of the LST in order to meet the net total of 30% addition of basanite to the ULST. Extrapolated temperatures from zoned sanidines within the outer carapace imply that the average storage temperatures of the magmas were low (630-670°C) and indicate that any high temperature episodes were not prolonged, no more that several hundred years (Rout and Wörner 2018). This would suggest that the hotter basanite magma was drip fed as small batches rather than larger volume events that would have resulted in larger changes to the temperature of the magma.

## 6. Conclusions

We present micro-beam major and trace element data for glasses from the Laacher See Tephra and reassess the petrogenesis of this zoned magmatic sequence. Fractional crystallisation remains a key process driving compositional gradients within the Laacher See Tephra, however our new data suggest that basanite recharge played an important role in the magmatic evolution of the ULST. This coupled fractionation and basanite recharge model is preferred to the previous studies that have argued that the compositional variations are solely related to fractionation on the basis of: 1) the consistency of mixing profiles across a range of elements; 2) the non-zero intercept of the highly incompatible elements on biplots; and 3) the mismatch between the degree of fractionation predicted by major and trace elements across the LST. In addition, basanite mixing offers an alternative explanation for the occurrence of oscillatory-zoned sanidines within the ULST and also for the less radiogenic <sup>87</sup>Sr/<sup>86</sup>Sr compositions in the ULST. We suggest that mafic recharge into the ULST caused an increase in the REE+Y and reduced the steepness of the U-shaped REE profile within the ULST. Mixing calculations indicate that the ULST magma was augmented by the addition of an average of 30% basanitic melt (range 10-50%), which was likely injected over 4-8 recharge events. Repeated episodes of basanite recharge into the ULST crystal mush extended the range of compositions, which could not be produced by fractionation alone. We suggest that basanite addition provided heat to the upper crust, driving strong thermal and compositional gradients and sustained the Laacher See magmatic system.

## Acknowledgements

This work was funded by the NERC RESET consortium (NE/E015905/1). The authors would like to thank Alice Williams for field assistance and Neil Holloway for sample polishing. We also gratefully acknowledge Chris Ballhaus for editorial handling, and Gerhard Wörner for a detailed and thorough review of this work.

## Table and figure captions

Table 1: Representative major and trace element composition of LST glasses determined by EMPA and LA-ICP-MS, \*compositions of basanite lavas were analysed by ICP-OES/MS. The full dataset is provided as Supplementary Information. <sup>s</sup>Hypothetical LST parent calculated by extrapolating the MLST+LLST trends to 500ppm Zr.

Figure 1: Stratigraphic section of the Laacher See Tephra (modified from Ginibre et al. (2004b) showing the three main stratigraphic units (LLST, MLST, ULST) and subunits (Bogaard and Schminke 1984) and the locations of studied samples within the stratigraphy.

Figure 2: Major element composition of LST glasses compared to (a,c,e) published whole rock data (Wörner et al. 1983b; Wörner and Schmincke 1984a; Wörner and Wright 1984); and (b, d, f) whole rock data for hybrid LST clasts (Wörner and Wright 1984) and East Eifel basanite lavas (this study; Wörner, Beusen, et al. 1983; Gluhak & Hofmeister 2009).

Figure 3: Average composition of LLST, MLST and ULST glasses: a) Trace elements normalised to primitive mantle (Sun and McDonough 1989); and b) Rare Earth Elements normalised to CI chondrite (McDonough and Sun 1995).

Figure 4: Trace element biplots showing composition of LST glasses compared published whole rock data (Wörner et al. 1983b; Wörner and Schmincke 1984a; Wörner and Wright 1984), hybrid clasts (Wörner and Wright 1984) and East Eifel basanite lavas (this study; Wörner, Beusen, et al. 1983; Gluhak & Hofmeister 2009).

Figure 5: Trace element biplots showing: (a-d) ULST glass compositions and pure titanite fractionation curve (blue) at intervals from 1 to 5% starting at the least evolved ULST glass composition calculated using the partition coefficients of (Olin and Wolff 2012) and (warm colours) the effect of variable proportions of titanite in a fractionating assemblage of feldspar (85%), clinopyroxene (8%) and amphibole (3%). (e-f) Calculated melt and residue trends in 10% increments produced by fractionation of REE-bearing phases from the MLST.

Figure 6: Compatible-incompatible element biplot for LST glasses showing fractionation trends calculated for a range of  $D_V$  values ( $D=2.6$  for the calculated ULST fractionation assemblage of (Wörner and Schmincke 1984b). The effect of combined fractionation and recharge is also indicated.

Figure 7: Incompatible-incompatible element mixing plots (left) and companion plots (right) after Langmuir et al. (1978) showing calculated mixing lines between the Rothenburg basanite and the least mixed ULST glass (LS10-3, green) and the hypothetical LST starting composition calculated by extrapolating the MLST+LLST

trends to 500ppm Zr (red), both plotted at 10% increments.

Figure 8: Schematic diagram showing proposed structure of the LST magmatic system.

## References

- Annen C (2009) From plutons to magma chambers: Thermal constraints on the accumulation of eruptible silicic magma in the upper crust. *Earth Planet Sci Lett* 284:409–416
- Baales M, Joris O, Street M, et al (2002) Impact of the late glacial eruption of the Laacher See volcano, Central Rhineland, Germany. *Quat Res* 58:273–288. doi: 10.1006/qres.2002.2379
- Bachmann O, Bergantz GW (2009) Rhyolites and their Source Mushes across Tectonic Settings. *J Petrol* 49:2277–2285. doi: 10.1093/petrology/egn068
- Bachmann O, Deering CD, Lipman PW, Plummer C (2014) Building zoned ignimbrites by recycling silicic cumulates: insight from the 1,000 km(3) Carpenter Ridge Tuff, CO. *Contrib to Mineral Petrol* 167:. doi: 10.1007/s00410-014-1025-3
- Bachmann O, Huber C (2016) Silicic magma reservoirs in the Earth's crust. *Am Mineral* 101:2377–2404. doi: 10.2138/am-2016-5675
- Bacon C, Druitt TH (1988) Compositional evolution of the zoned calcalkaline magma chamber of Mount Mazama, Crater Lake, Oregon. *Contrib to Mineral Petrol* 98:224–256
- Barboni M, Boehnke P, Schmitt AK, et al (2016) Warm storage for arc magmas. *Proc Natl Acad Sci* 113:13959 LP – 13964. doi: 10.1073/pnas.1616129113
- Berndt J, Holtz F, Koepke J (2001) Experimental constraints on storage conditions in the chemically zoned phonolitic magma chamber of the Laacher See volcano. *Contrib to Mineral Petrol* 140:469–486. doi: 10.1007/pl00007674
- Bogaard P, Schmincke HU (1985) Laacher See Tephra - a widespread isochronous late quaternary tephra layer in central and northern Europe. *Geol Soc Am Bull* 96:1554–1571. doi: 10.1130/0016-7606(1985)96<1554:lstawi>2.0.co;2
- Bogaard P, Schmincke HU (1984) The eruptive center of the later Quaternary Laacher See Tephra. *Geol Rundschau* 73:933–980
- Bourdon B, Zindler A, Worner G (1994) Evolution of the Laacher-See magma chamber - evidence from SIMS and TIMS measurements of U-Th disequilibria in minerals and glasses. *Earth Planet Sci Lett* 126:75–90. doi: 10.1016/0012-821x(94)90243-7
- Brauer A, Endres C, Negendank JFW (1999) Lateglacial calendar year chronology based on annually laminated sediments from Lake Meerfelder Maar, Germany. *Quat Int* 61:17–25. doi: 10.1016/s1040-6182(99)00014-2
- Cashman K V, Sparks RSJ, Blundy JD (2017) Vertically extensive and unstable magmatic systems: A unified view of igneous processes. *Science* (80- ) 355:. doi: 10.1126/science.aag3055
- Coombs DS, Wilkinson JFG (1969) Lineages and Fractionation Trends in Undersaturated Volcanic Rocks from the East Otago Volcanic Province (New Zealand) and Related Rocks. *J Petrol* 10:440–501. doi: 10.1093/petrology/10.3.440
- Cooper KM, Kent AJR (2014) Rapid remobilization of magmatic crystals kept in cold storage. *Nature* 506:480
- Deering CD, Bachmann O, Vogel TA (2011) The Ammonia Tanks Tuff: Erupting a melt-rich rhyolite cap and its remobilized crystal cumulate. *Earth Planet Sci Lett* 310:518–525. doi:

- <https://doi.org/10.1016/j.epsl.2011.08.032>
- Degruyter W, Huber C, Bachmann O, et al (2016) Magma reservoir response to transient recharge events: The case of Santorini volcano (Greece). *Geology* 44:23–26. doi: 10.1130/G37333.1
- Duda A, Schmincke H (1987) Quaternary basanites, melilitite nephelinites and tephrites from the Laacher See Area, Germany. *Neues Jahrb für Mineral* 132:1–33
- Dufek J, Bachmann O (2010) c. *Geology* 38:687–690. doi: 10.1130/G30831.1
- Eichelberger JC, Chertkoff DG, Dreher ST, Nye CJ (2000) Magmas in collision: Rethinking chemical zonation in silicic magmas. *Geology* 28:603–606. doi: 10.1130/0091-7613(2000)28<603:MICRCZ>2.0.CO;2
- Fedele L, Lustrino M, Melluso L, et al (2015) Trace-element partitioning between plagioclase, alkali feldspar, Ti-magnetite, biotite, apatite, and evolved potassic liquids from Campi Flegrei (Southern Italy). *Am Mineral* 100:233–249. doi: 10.2138/am-2015-4995
- Forni F, Petricca E, Bachmann O, et al (2018) The role of magma mixing/mingling and cumulate melting in the Neapolitan Yellow Tuff caldera-forming eruption (Campi Flegrei, Southern Italy). *Contrib to Mineral Petrol* 173:45. doi: 10.1007/s00410-018-1471-4
- Ganne J, Bachmann O, Feng X (2018) Deep into magma plumbing systems: Interrogating the crystal cargo of volcanic deposits. *Geology* 46:415–418. doi: 10.1130/G39857.1
- Gelman SE, Gutiérrez FJ, Bachmann O (2013) On the longevity of large upper crustal silicic magma reservoirs. *Geology* 41:759–762. doi: 10.1130/G34241.1
- Ginibre C, Davidson JP, Worner G (2004a) Sr isotope zoning in feldspars at Laacher See Volcano, Germany. *Geochim Cosmochim Acta* 68:A654–A654
- Ginibre C, Worner G, Kronz A (2004b) Structure and dynamics of the Laacher See magma chamber (Eifel, Germany) from major and trace element zoning in sanidine: A cathodoluminescence and electron microprobe study. *J Petrol* 45:2197–2223. doi: 10.1093/petrology/egh053
- Gluhak TM, Hofmeister W (2009) Roman lava quarries in the Eifel region (Germany): geochemical data for millstone provenance studies. *J Archaeol Sci* 36:1774–1782. doi: <https://doi.org/10.1016/j.jas.2009.04.007>
- Harms E, Gardner JE, Schmincke HU (2004) Phase equilibria of the Lower Laacher See Tephra (East Eifel, Germany): constraints on pre-eruptive storage conditions of a phonolitic magma reservoir. *J Volcanol Geotherm Res* 134:125–138. doi: 10.1016/j.jvolgeores.2004.01.009
- Harms E, Schmincke HU (2000) Volatile composition of the phonolitic Laacher See magma (12,900 yr BP): implications for syn-eruptive degassing of S, F, Cl and H<sub>2</sub>O. *Contrib to Mineral Petrol* 138:84–98. doi: 10.1007/PL00007665
- Hensch M, Dahm T, Ritter J, et al (2019) Deep low-frequency earthquakes reveal ongoing magmatic recharge beneath Laacher See Volcano (Eifel, Germany). *Geophys J Int* 216:2025–2036. doi: 10.1093/gji/ggy532
- Hildreth W, Wilson CJN (2007) Compositional Zoning of the Bishop Tuff. *J Petrol* 48:951–999. doi: 10.1093/petrology/egm007
- Humphreys MCS, Blundy JD, Sparks RSJ (2006) Magma evolution and open-system processes at Shiveluch Volcano: Insights from phenocryst zoning. *J Petrol* 47:2303–2334. doi: 10.1093/petrology/egl045
- Irving AJ, Green DH (2008) Phase relationships of hydrous alkalic magmas at high pressures: Production of nepheline hawaiitic to mugearitic liquids by amphibole-dominated fractional crystallization within the lithospheric mantle. *J Petrol* 49:741–756. doi: 10.1093/petrology/egm088
- Irving AJ, Price RC (1981) Geochemistry and evolution of Iherzolite-bearing phonolitic lavas from Nigeria, Australia, East Germany and New Zealand. *Geochim Cosmochim Acta* 45:1309–1320. doi: [https://doi.org/10.1016/0016-7037\(81\)90224-6](https://doi.org/10.1016/0016-7037(81)90224-6)



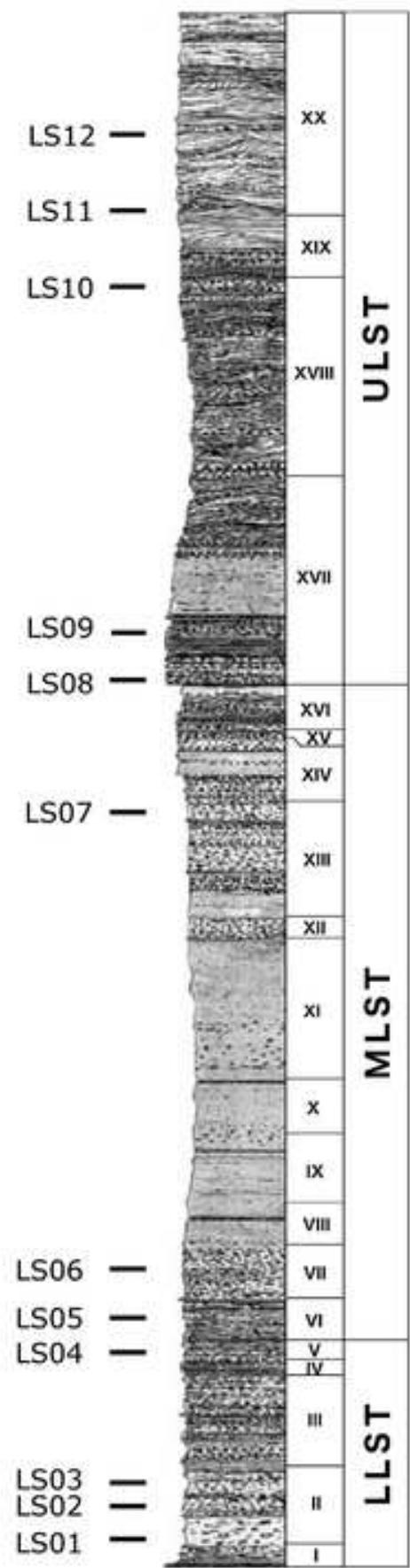
- Jochum K ~P., Stoll B, Herwig K, et al (2006) MPI-DING reference glasses for in situ microanalysis: New reference values for element concentrations and isotope ratios. *Geochemistry, Geophys Geosystems* 7:Q02008. doi: 10.1029/2005GC001060
- Langmuir CH, Vocke RD, Hanson GN, Hart SR (1978) General mixing equation with applications to Icelandic basalts. *Earth Planet Sci Lett* 37:380–392. doi: 10.1016/0012-821X(78)90053-5
- Le Roex AP, Cliff RA, Adair BJI (1990) Tristan-da-Cunha, south-Atlantic - geochemistry and petrogenesis of a basanite phonolite lava series. *J Petrol* 31:779–812. doi: 10.1093/petrology/31.4.779
- Lisewska KM, White JC, Macdonald R, Bagiński B (2018) Compositional and Thermodynamic Variability in a Stratified Magma Chamber: Evidence from the Green Tuff Ignimbrite (Pantelleria, Italy). *J Petrol* 59:2245–2272. doi: 10.1093/petrology/egy095
- Litt T, Schmincke HU, Kromer B (2003) Environmental response to climatic and volcanic events in central Europe during the Weichselian Lateglacial. *Quat Sci Rev* 22:7–32. doi: 10.1016/s0277-3791(02)00180-4
- Masotta M, Freda C, Gaeta M (2012) Origin of crystal-poor, differentiated magmas: insights from thermal gradient experiments. *Contrib to Mineral Petrol* 163:49–65
- McDonough WF, Sun SS (1995) The composition of the Earth. *Chem Geol* 120:223–253. doi: 10.1016/0009-2541(94)00140-4
- Newhall CG, Self S (1982) The volcanic explosivity index (VEI) - an estimate of explosive magnitude for historical volcanism. *J Geophys Res* 87:1231–1238. doi: 10.1029/JC087iC02p01231
- Olin PH, Wolff JA (2012) Partitioning of rare earth and high field strength elements between titanite and phonolitic liquid. *Lithos* 128–131:46–54. doi: <https://doi.org/10.1016/j.lithos.2011.10.007>
- Rout SS, Worner G (2018) Zoning and exsolution in alkali feldspars from Laacher See volcano (Western Germany): constraints on temperature history prior to eruption. *Contrib to Mineral Petrol* 173:. doi: 10.1007/s00410-018-1522-x
- Schmitt AK (2006) Laacher See revisited: High-spatial-resolution zircon dating indicates rapid formation of a zoned magma chamber. *Geology* 34:597–600. doi: 10.1130/G22533.1
- Schmitt AK, Wetzel F, Cooper KM, et al (2010) Magmatic Longevity of Laacher See Volcano (Eifel, Germany) Indicated by U-Th Dating of Intrusive Carbonatites. *J Petrol* 51:1053–1085. doi: 10.1093/petrology/egq011
- Smith VC, Blundy JD, Arce JL (2009) A Temporal Record of Magma Accumulation and Evolution beneath Nevado de Toluca, Mexico, Preserved in Plagioclase Phenocrysts. *J Petrol* 50:405–426. doi: 10.1093/petrology/egp005
- Solano JMS, Jackson MD, Sparks RSJ, et al (2012) Melt Segregation in Deep Crustal Hot Zones: a Mechanism for Chemical Differentiation, Crustal Assimilation and the Formation of Evolved Magmas. *J Petrol* 53:1999–2026. doi: 10.1093/petrology/egs041
- Sun S-S, McDonough WF (1989) Chemical and isotopic systematics of oceanic basalts: implications for mantle composition and processes. In: Saunders AD, Norry MJ (eds) *Magmatism in Ocean Basins*. Geol. Soc. Spec. Publ., London, pp 313–345
- Tait SR, Worner G, Vandembogaard P, Schmincke HU (1989) Cumulate nodules as evidence for convective fractionation in a phonolite magma chamber. *J Volcanol Geotherm Res* 37:21–37. doi: 10.1016/0377-0273(89)90111-x
- Tomlinson EL, Thordarson T, Müller W, et al (2010) Microanalysis of tephra by LA-ICP-MS - Strategies, advantages and limitations assessed using the Thorsmork ignimbrite (Southern Iceland). *Chem Geol* 279:73–89. doi: 10.1016/j.chemgeo.2010.09.013

766 Wolff JA, Ellis BS, Ramos FC, et al (2015) Remelting of cumulates as a process for producing chemical zoning  
767 in silicic tuffs: A comparison of cool, wet and hot, dry rhyolitic magma systems. *Lithos* 236–237:275–286.  
768 doi: <https://doi.org/10.1016/j.lithos.2015.09.002>

1 769 Worner G, Beusen JM, Duchateau N, et al (1983a) Trace-element abundances and mineral melt distribution  
2 coefficients in phonolites from the Laacher-See volcano (Germany). *Contrib to Mineral Petrol* 84:152–173  
3 770  
4 771 Worner G, Schmincke HU (1984a) Mineralogical and chemical zonation of the laacher see tephra sequence (East  
5 Eifel, West-Germany). *J Petrol* 25:805–835. doi: 10.1093/petrology/25.4.805  
6 772  
7 773 Worner G, Schmincke HU (1984b) Petrogenesis of the zoned Laacher See tephra. *J Petrol* 25:836–851. doi:  
8 10.1093/petrology/25.4.836  
9 774  
10 775 Worner G, Schmincke HU, Wright TL (1983b) Evidence for magma mixing within the Laacher See magma  
11 chamber (East Eifel). *Fortschritte Der Mineral* 61:220–221  
12 776  
13 777 Worner G, Staudigel H, Zindler A (1985) Isotopic constraints on open system evolution of the Laacher-See  
14 magma chamber (Eifel, West-Germany). *Earth Planet Sci Lett* 75:37–49. doi: 10.1016/0012-  
15 821x(85)90048-2  
16 778  
17 779  
18 780 Worner G, Wright TL (1984) Evidence for magma mixing within the Laacher See magma chamber (East-Eifel,  
19 Germany). *J Volcanol Geotherm Res* 22:301–327. doi: 10.1016/0377-0273(84)90007-6  
20 781  
21 782

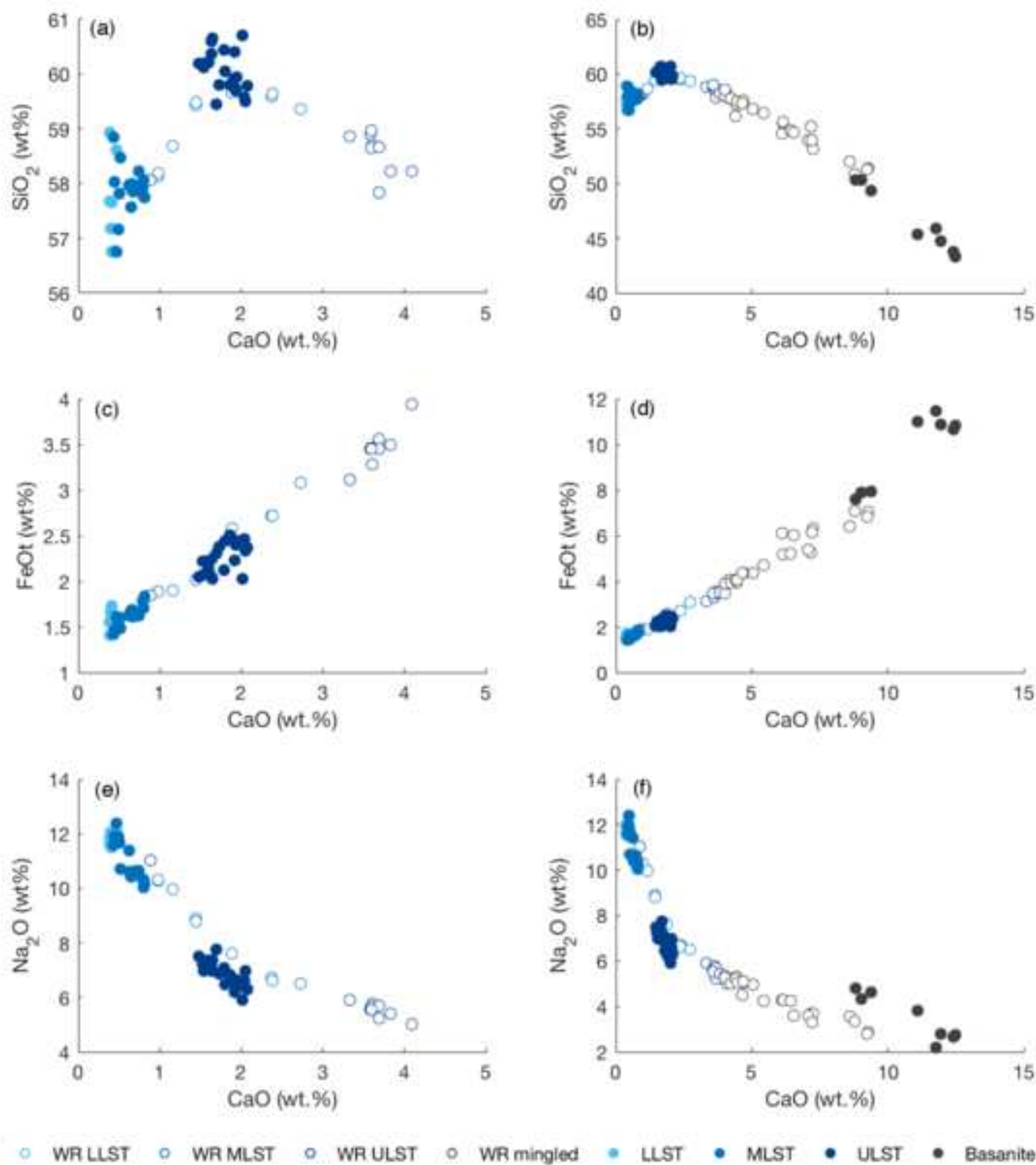
Figure

[Click here to access/download;Figure;fig1.png](#)



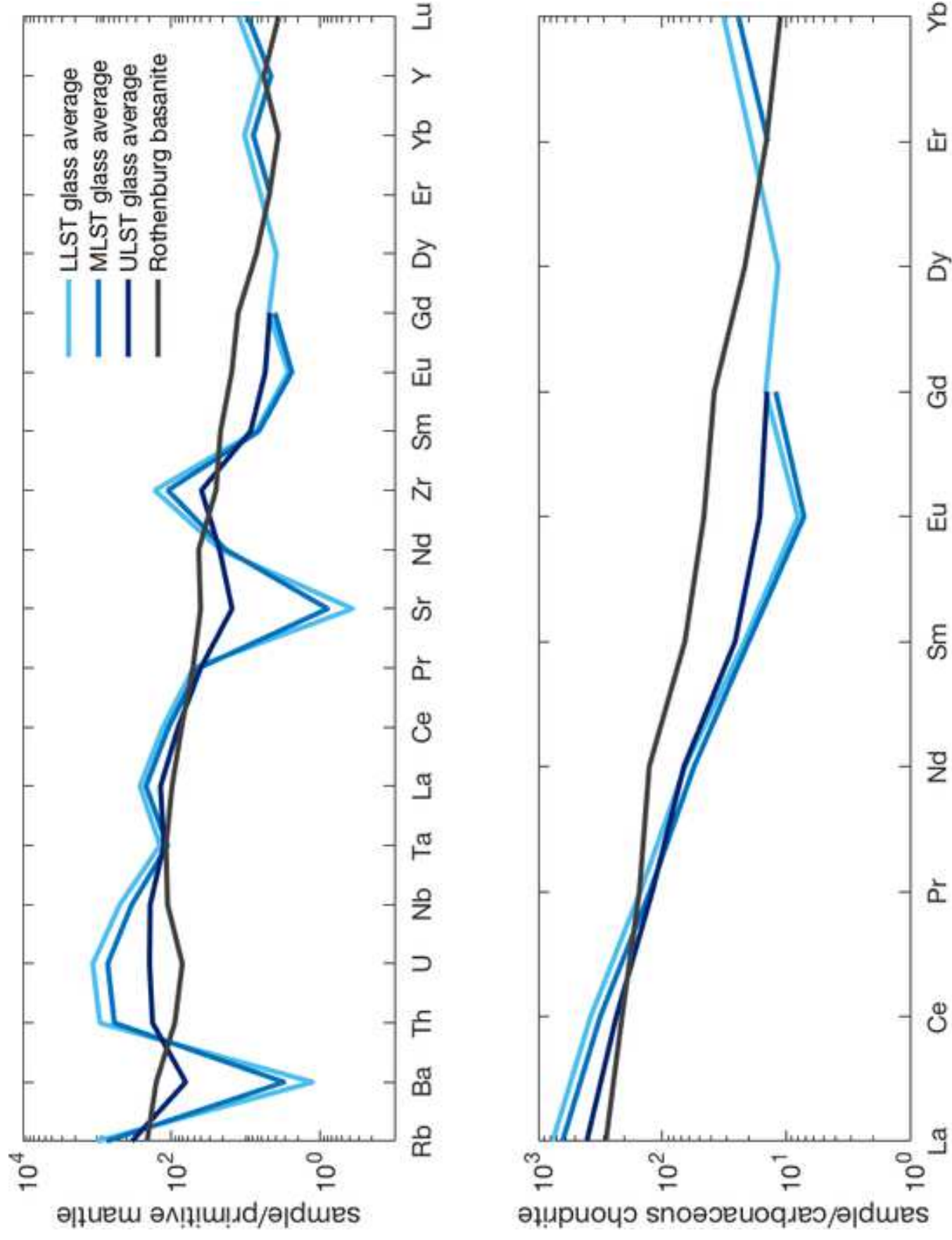
Figure

[Click here to access/download;Figure;Fig2.png](#)



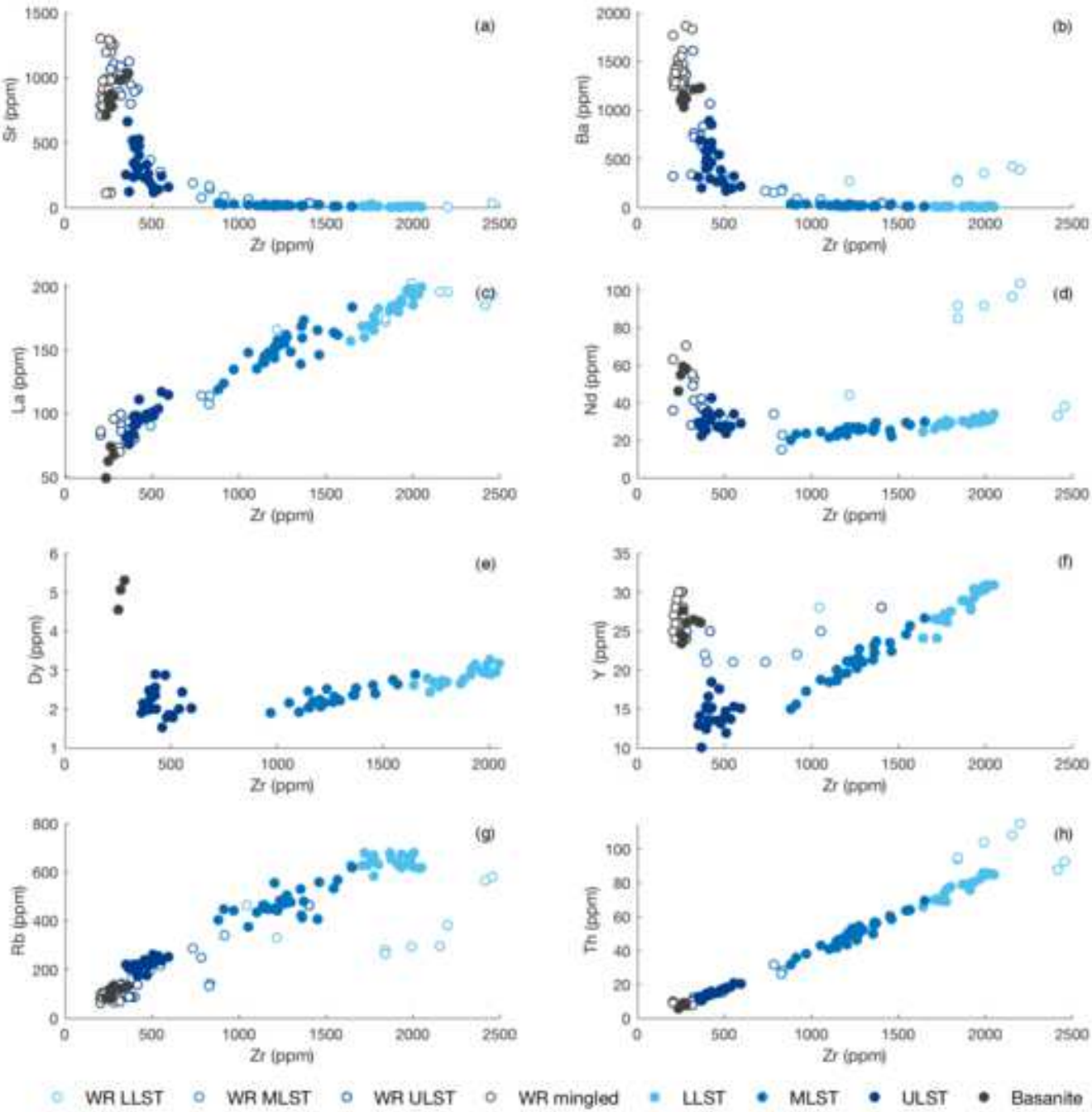
Figure

[Click here to access/download;Figure;Fig3.png](#)

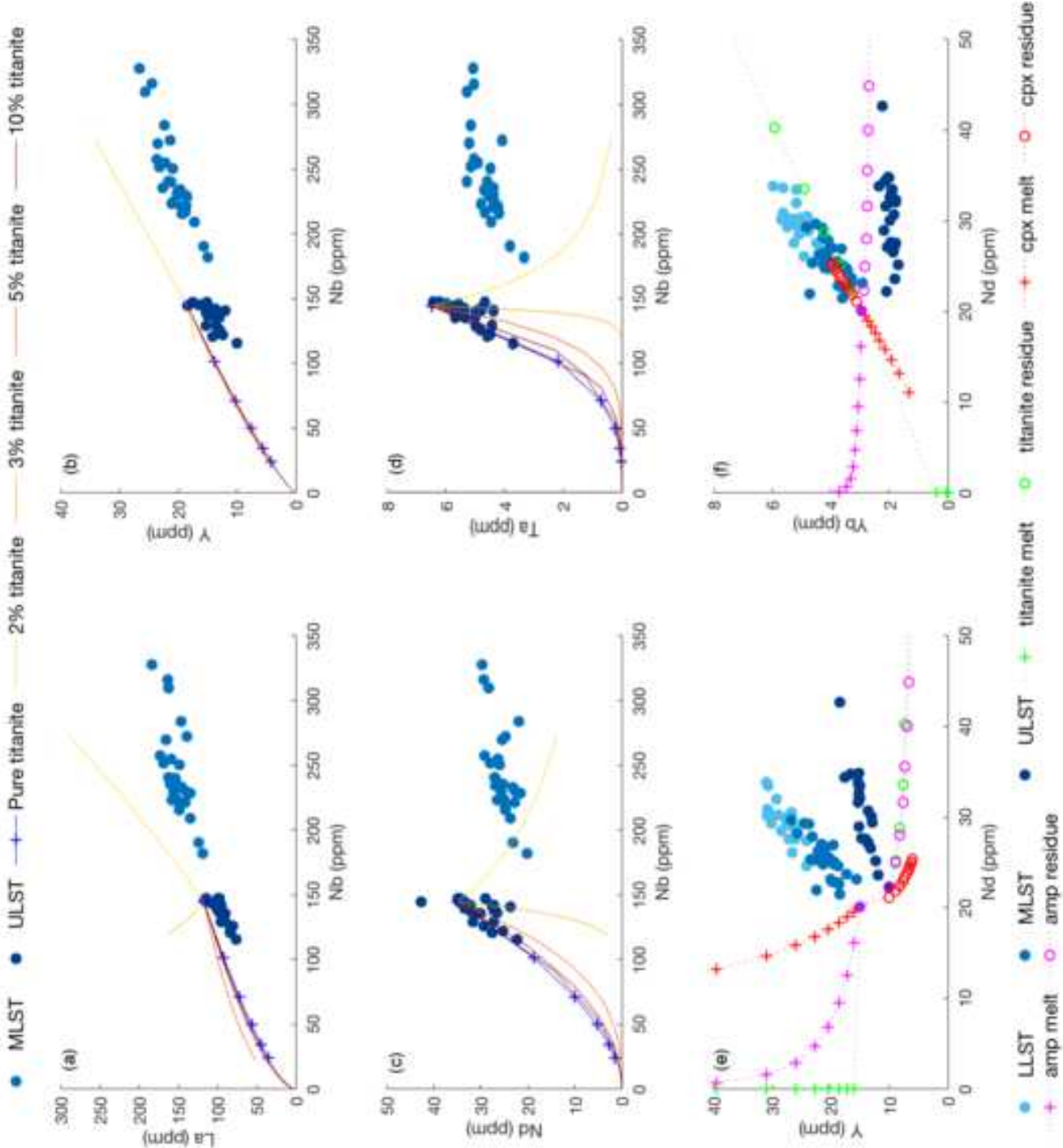


Figure

[Click here to access/download;Figure;Fig4.png](#)



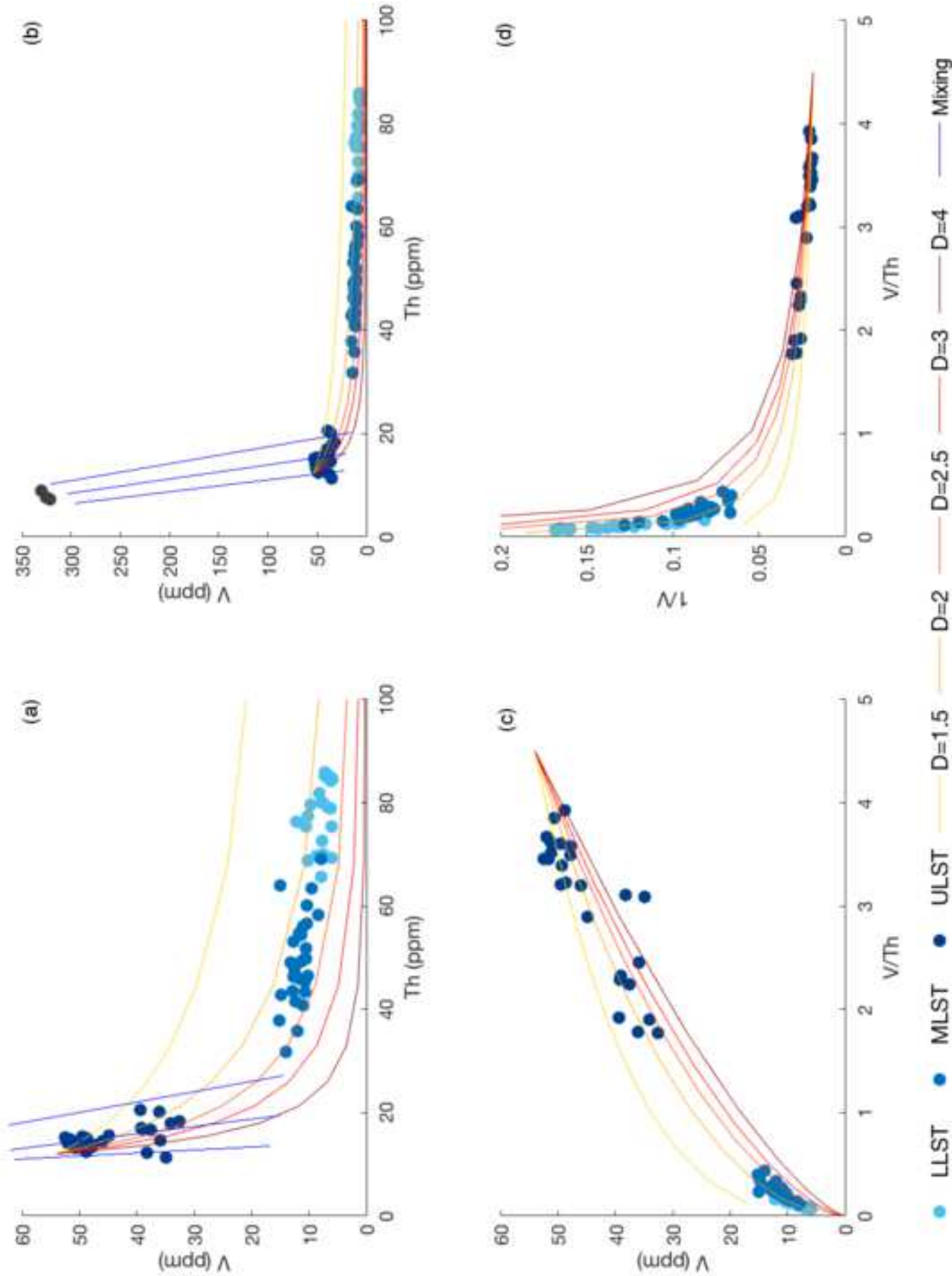
Figure





Figure

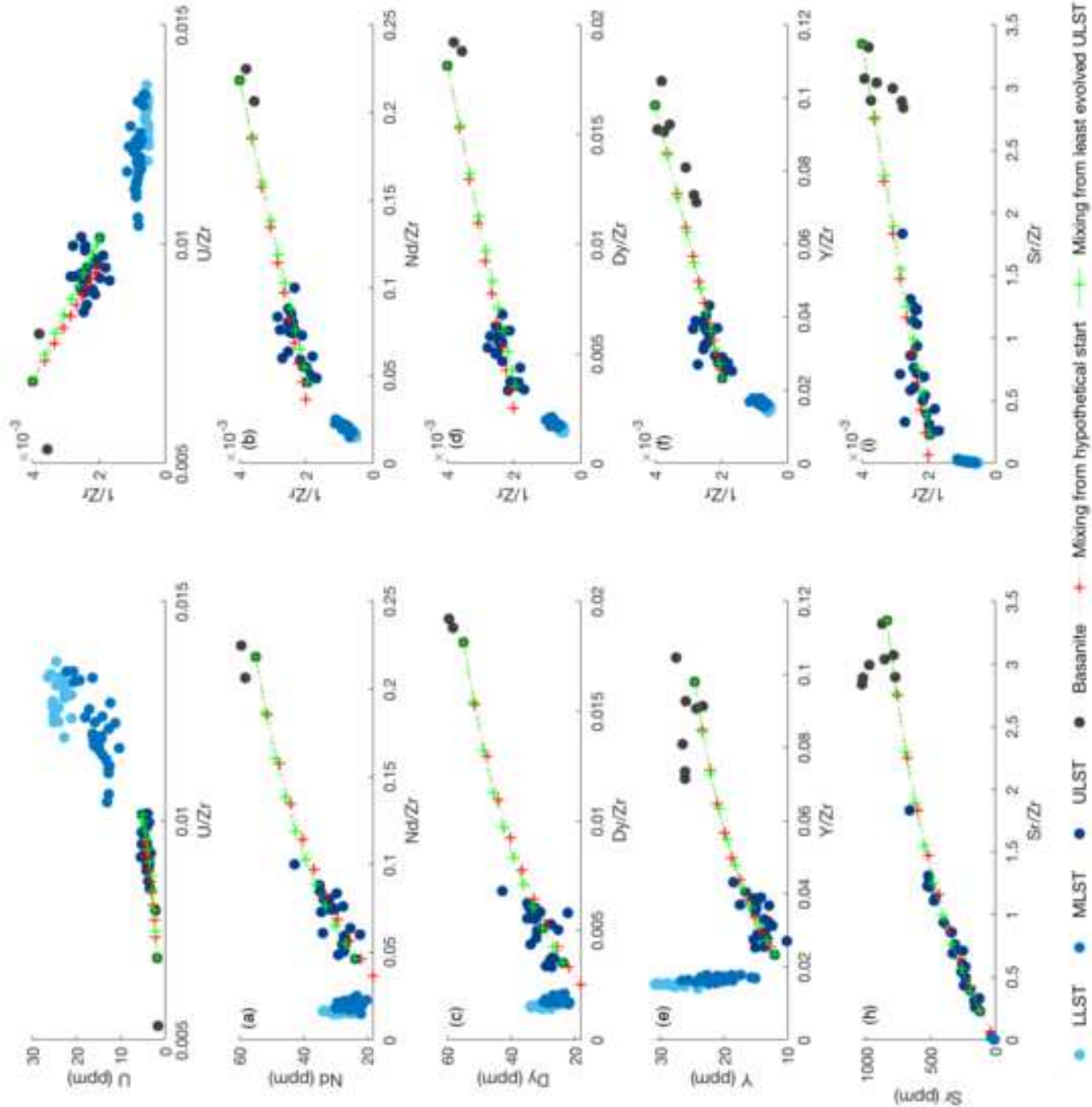
[Click here to access/download;Figure;Fig6.png](#)





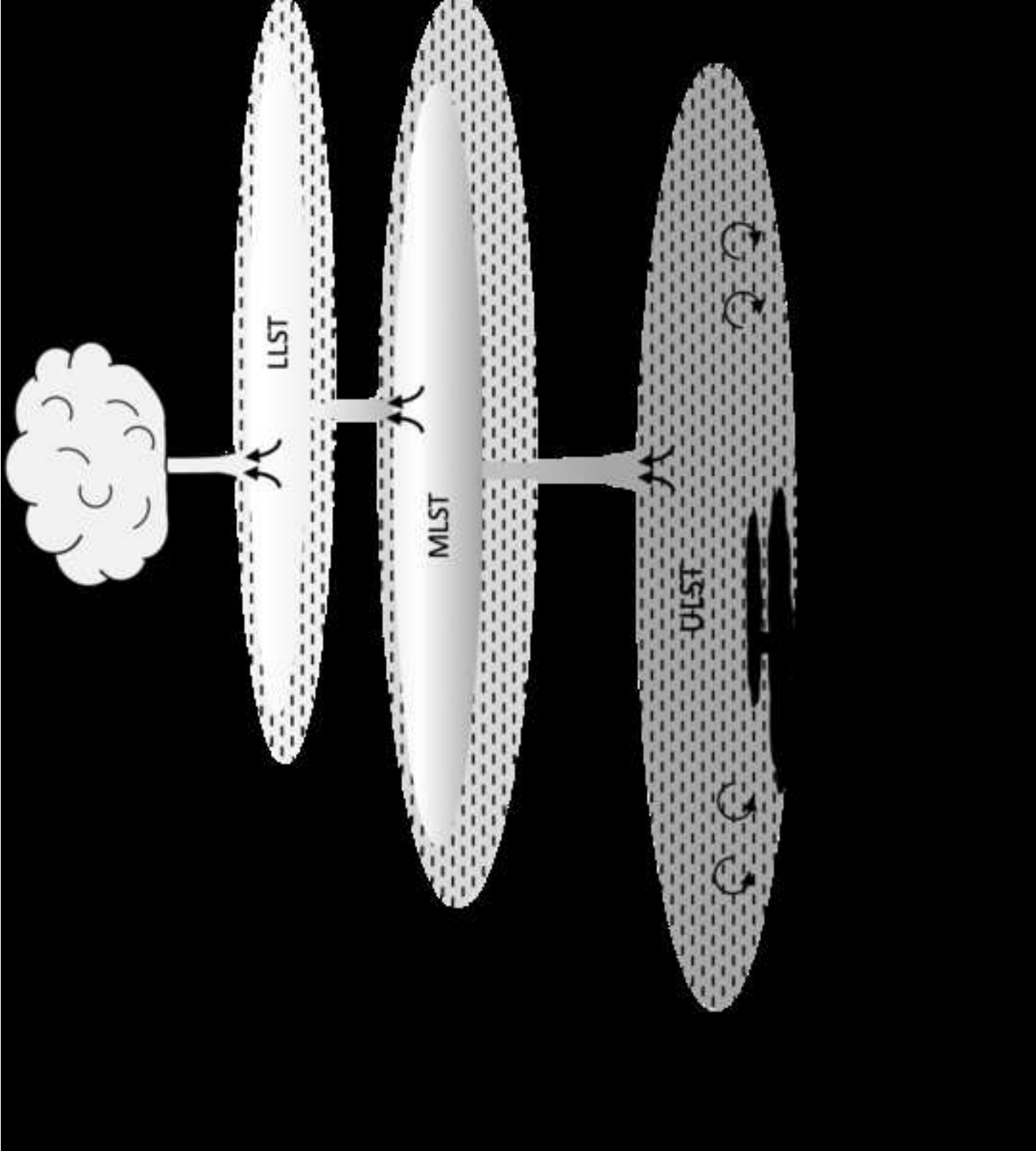
Figure

[Click here to access/download;Figure;Fig7.png](#)



Figure

[Click here to access/download;Figure;Fig8.png](#)



Unit	LS1	LS2	LS3	LS4	LS5	LS6	LS7	LS8	LS9	LS10	LS11	LS12	Basanit <sup>e</sup> LS09	Basanit <sup>e</sup> Rothen- berg*	Hypoth- etical LST parent <sup>s</sup>
Sample	LS01	LS02	LS03	LS04	LS05	LS06	LS07	LS08	LS09	LS10	LS11	LS12	LS09	Rothen- berg*	LST
Analysis	LS01-12	LS02-21	LS03-6	LS04-22	LS05-13	LS06-23	LS07-27	LS08-1	LS09-27	LS10-2	LS11-13	LS12-22	lithic*	berg*	parent <sup>s</sup>
Major element (wt% oxide)															
SiO2	58.94	57.65	57.17	58.62	58.02	57.82	57.93	60.19	60.19	59.80	59.73	59.69	45.85	44.74	
TiO2	0.11	0.11	0.15	0.08	0.11	0.14	0.18	0.38	0.42	0.56	0.56	0.59	2.65	2.60	
Al2O3	21.98	22.71	22.69	22.09	22.46	22.26	22.35	20.87	20.37	20.27	20.40	20.30	14.58	13.59	
FeO <sup>t</sup>	1.41	1.55	1.58	1.50	1.46	1.61	1.78	2.07	2.21	2.38	2.45	2.40	11.47	10.86	
MnO	0.45	0.52	0.63	0.48	0.43	0.46	0.32	0.18	0.22	0.22	0.15	0.15	0.17	0.17	
MgO	0.02	0.02	0.02	0.05	0.03	0.02	0.05	0.20	0.22	0.28	0.30	0.32	7.41	9.33	
CaO	0.39	0.41	0.40	0.46	0.45	0.51	0.79	1.52	1.53	1.73	1.93	1.93	11.76	11.94	
Na2O	11.59	11.50	12.06	12.06	11.93	11.67	10.33	7.38	7.21	6.88	6.64	6.58	2.21	2.77	
K2O	4.93	5.14	4.94	4.38	4.67	5.18	5.83	6.80	7.25	7.48	7.49	7.70	3.16	3.29	
P2O5	0.00	0.04	0.00	0.09	0.00	0.00	0.01	0.05	0.06	0.07	0.07	0.07	0.56	0.52	
Cl	0.19	0.33	0.36	0.18	0.43	0.34	0.42	0.35	0.32	0.33	0.28	0.28	-	-	
Total	96.00	90.06	94.29	99.11	98.51	94.68	94.39	95.96	96.25	97.93	97.75	98.07	99.82	99.82	
Trace element (ppm)															
Rb	671	655	664	668	532	464	441	219	205	251	213	235	135	82	215
Sr	4.3	9.0	2.6	9.2	7.2	14.8	25.2	255	345	156	260	242	854	840	33
Y	29.3	30.7	30.7	26.8	24.5	18.7	17.3	15.2	13.0	15.1	13.1	15.3	26.1	24.6	13
Zr	1937	1987	1990	1776	1547	1141	971	417	401	597	479	555	281	251	500
Nb	350	366	365	352	316	221	209	140	136	147	136	146	80	77	130
Ba	5.5	6.2	2.6	11.3	14.5	19.3	32.0	295	503	217	386	322	1117	1091	40
La	187	199	194	166	164	141	135	96	90	115	98	117	67	63	103
Ce	234	258	243	217	211	180	175	149	139	156	138	157	129	119	132
Pr	13.7	15.6	15.2	12.7	12.1	10.5	11.0	11.9	11.1	11.2	10.2	11.9	14.1	13.4	8.3
Nd	32.0	33.5	33.6	30.5	29.3	22.8	23.7	33.4	30.0	29.0	26.6	33.8	58.1	54.8	12.2
Sm	<LOD	<LOD	3.2	<LOD	<LOD	<LOD	<LOD	<LOD	4.0	<LOD	2.9	3.8	9.7	9.2	2.6
Eu	<LOD	<LOD	0.5	<LOD	<LOD	<LOD	<LOD	0.8	1.0	0.7	0.7	1.0	2.6	2.5	-
Gd	<LOD	<LOD	2.9	<LOD	<LOD	<LOD	<LOD	<LOD	<LOD	<LOD	1.9	3.3	7.5	7.2	-
Dy	3.1	2.9	3.1	2.6	2.7	<LOD	1.9	2.3	2.0	2.0	1.8	2.4	5.3	4.5	1.3
Er	3.1	3.2	3.2	2.7	2.8	2.1	1.8	1.9	1.5	1.6	1.3	1.4	2.3	2.3	1.3
Yb	5.2	5.2	5.6	4.8	4.8	3.7	3.3	1.9	2.0	2.2	1.9	2.4	1.8	1.7	2.0
Lu	0.9	1.1	1.0	0.7	0.7	0.6	0.5	<LOD	<LOD	0.4	0.3	0.5	0.3	0.2	0.4
Ta	5.9	6.4	5.9	5.7	5.1	4.2	4.5	5.0	5.3	4.7	5.0	5.6	4.8	4.8	3.4
Th	80	86	85	69	63	44	38	14.5	13.1	20.2	16.8	20.5	7.6	7.2	17.5
U	25.8	26.4	25.3	23.2	20.7	12.8	12.3	4.1	3.6	5.5	4.6	5.2	1.5	1.7	4.8